Ultrafast Isomerization Initiated by X-Ray Core Ionization

Chelsea E. Liekhus-Schmaltz[1,2], Ian Tenney[1,2], Timur Osipov[3], Alvaro Sanchez-Gonzalez[4], Nora Berrah[3], Rebecca Boll[5,6], Cedric Bomme[5], Christoph Bostedt[7], John D. Bozek[7], Sebastian Carron[7], Ryan Coffee[7], Julien Devin[1,2], Benjamin Erk[5], Ken R. Ferguson[7,8], Robert W. Field[9], Lutz Foucar[10], Leszek J. Frasinski[4], James M. Glownia[7], Markus Gühr[2], Andrei Kamalov[1,2], Jacek Krzywinski[7], Heng Li[2,7], Jonathan P. Marangos[4], Todd J. Martinez[2,11], Brian K. McFarland[2], Shungo Miyabe[2,11], Brendan Murphy[3], Adi Natan[2], Daniel Rolles[5], Artem Rudenko[12], Marco Siano[4], Emma R. Simpson[4], Limor Spector[1,2], Michele Swiggers[7], Daniel Walke[4], Song Wang[1,2], Thorsten Weber[13], Philip H. Bucksbaum[1,2,8], Vladimir S. Petrovic[1,2,*]

[1]*Department of Physics, Stanford University, 382 Via Pueblo Mall, Stanford, CA 94305*

[2]*PULSE Institute for Ultrafast Energy Science, 2575 Sand Hill Road, Menlo Park, CA 94025*

[3]*Department of Physics, University of Connecticut, 2152 Hillside Road, Storrs, CT 06269*

[4]*Department of Physics, Imperial College London, Prince Consort Road, London SW7 2AZ, United Kingdom*

[5]*Deutsches Elektronen-Synchrotron, Notkestrasse 85, 22607 Hamburg, Germany*

[6]*Max Planck Institute for Nuclear Physics, Saupfercheckweg 1, 69117 Heidelberg, Germany*

[7]*Linac Coherent Light Source, 2575 Sand Hill Road, Menlo Park, CA 94025*

[8]*Department of Applied Physics, 382 Via Pueblo Mall, Stanford University, Stanford, CA 94305*

[9]*Department of Chemistry, Massachusetts Institute of Technology, 77 Massachusetts Avenue, Cambridge, MA 02139*

[*]petrovic@slac.stanford.edu

[10]*Max Planck Institute for Medical Research, Jahnstrasse 29, 69120 Heidelberg, Germany*

[11]*Department of Chemistry, Stanford University, 333 Campus Drive, Stanford, CA 94305*

[12]*J. R. Macdonald Laboratory, Department of Physics, 306 Cardwell Hall, Kansas State University, Manhattan, KS 66506*

[13]*Lawrence Berkeley National Lab, 1 Cyclotron Road, Berkeley, CA 94720*

Rapid proton migration is a key process in hydrocarbon photochemistry. Charge migration and subsequent proton motion can mitigate radiation damage when heavier atoms absorb x-rays. If rapid enough this can improve the fidelity of diffract-before-destroy measurements of biomolecular structure at x-ray free electron lasers. We have studied x-ray-initiated isomerization of acetylene, a model for proton dynamics in hydrocarbons. Our time-resolved measurements capture the transient motion of protons following x-ray ionization of carbon K-shell electrons. We Coulomb-explode the molecule with a second precisely delayed x-ray pulse and then record all the fragment momenta. These snapshots at different delays have been combined into a 'molecular movie' of the evolving molecule, which shows substantial proton redistribution within the first 12 femotseconds. We conclude that significant proton motion occurs on a timescale comparable to the Auger relaxation that refills the K-shell vacancy.

Introduction

Proton migration in the acetylene dication has received significant attention as a model for understanding isomerization driven by nonadiabatic electron-nuclear interactions in more complex

organic materials. Measurements reported by Osipov et al. indicate that, when initiated by x-ray core ionization, this isomerization can occur on a timescale shorter than 60 fs[1,2]. This ultrafast rate was unexpected based on the predicted barrier heights in the electronic states populated in relaxation upon core ionization[3,4]. We investigated this process in a time-resolved x-ray pump/x-ray probe experiment at Linac Coherent Light Source (LCLS), a free electron laser (FEL) x-ray source at SLAC National Accelerator Laboratory. This new technique allows direct probing of the isomerization in the time domain.

X-ray free electron lasers can produce intense femtosecond pulses of coherent x-rays. These light sources have been employed for molecular and material science, as well as structural biology[6,7,10–18]. Current and future x-ray FELs plan to deliver ultrashort x-ray pulses with sufficiently high intensity to collect diffraction images of selected targets in a single shot. This prospect of nearly instantaneous diffraction-before-destruction is motivating a dedicated research effort at x-ray FELs[19–21].

Single-particle diffraction requires an x-ray pulse duration shorter than the timescale associated with the radiation damage[6,7,22–24]. Core-ionization and subsequent Auger decay in intense x-ray fields creates a highly charged molecule that eventually falls apart by Coulomb repulsion. The small mass of protons makes intramolecular proton migration the fastest nuclear response to the significant disruption of the electronic structure caused by the x-ray ionization. The acetylene dication is the smallest hydrocarbon that can isomerize and is thus a prototype for investigations of the electronic-nuclear nonadiabatic interactions that underlie basic unimolecular isomerization and radiation damage of biological material, relevant for diffraction-before-destruction techniques and

in vivo radio-oncology[25]. The nonadiabatic interactions that hinder the separation of the electronic and nuclear motion in molecules under certain conditions cause the Born-Oppenheimer approximation to break down and require advanced quantum computational techniques for treatment[26].

Isomerization of acetylene HCCH to form vinylidene H_2CC has been studied in the neutral molecule, as well as singly and doubly charged acetylene ions[1,2,27–39]. Acetylene cations are important not only as a model for molecular dynamics and radiation damage investigations, but also in a range of applications, from plasma devices[40], combustion[41], semiconductor manufacturing[42], to understanding planetary atmospheres[43]. Isomerization of the dication has been investigated in synchrotron experiments[1,2,30,31,37]. Osipov et al. performed ion-ion-photoelectron and ion-ion-Auger electron coincidence measurements to study the fragmentation of the dication formed upon core-ionization of acetylene[1,2]. These measurements place an upper limit of 60 fs on the time for the x-ray initiated isomerization[1,2]. Osipov et al. proposed that the isomerization occurs on the lowest singlet state of the dication $^1\Sigma_g^+$ (see Fig. 1), although participation of the $^1\Delta_g$ state could not be ruled out[2]. Calculations[3,4] predict the barrier for the isomerization on the $^1\Sigma_g^+$ potential energy surface to be 2.3 eV. At the same time, the vibrational excitation of the acetylene dication after Auger decay is expected to be smaller than the barrier height[2]. This would imply isomerization times on the picosecond timescale according to transition-state theory[4]. The mechanism of the unexpectedly fast isomerization could not be probed by the measurements reported in Refs. [1] and [2] because they were not time-resolved. This process has been studied in time-resolved optical laser experiments coupled with three- and four-particle coincident detection [33,35,36,39].

Optical laser experiments find that deuterium migrates to form vinylidene on a timescale of $\sim$ 90 fs when strong-field 800 nm radiation initiates isomerization. In the singly-charged ion the ultrafast isomerization is not launched with 800 nm radiation, but has been demonstrated to proceed from the excited $A^2\Sigma_g^+$ state [29,38]. Core-ionization, which was employed in the current work for initiating isomerization, occurs in the weak field regime, unlike the strong-field 800 nm experiments. Core ionization, followed by Auger relaxation, results in a different distribution of dicationic states and a different degree of vibrational excitation than strong-field ionization. The isomerization mechanism can differ between these two cases.

To measure the ultrafast timescale of this prototypical x-ray initiated isomerization, we performed a time-resolved x-ray pump/x-ray probe experiment at LCLS that directly detected the geometry change in $C_2D_2^{2+}$. $C_2D_2^{2+}$ rather than $C_2H_2^{2+}$ is employed to eliminate potential background sources of protons from water or other contaminants. Although the two molecules have the same electronic structure, if the isomerization rate is limited by the nuclear masses, one would expect both the particle velocity and the rate of the tunneling through the barrier to be slower in $C_2D_2^{2+}$ compared to $C_2H_2^{2+}$.

Our measurements indicate that the isomerization in the deuterated acetylene dication already begins in the first 12 fs following core ionization. This finding is consistent with a non-static geometry prior to the Auger transition. As suggested by Gadea et al. [5], when lighter nuclei are involved, molecular geometry can begin to evolve during the core-hole lifetime. This geometry change during the core-hole excitation, which is typically neglected in the analysis of core-

ionization experiments, implies that transition-state theory applied to the potential energy surface of the dication alone is insufficient to account for the ultrafast proton migration[4]. This new result will inform realistic models of radiation damage of biomaterials in single-molecule diffraction experiments at FEL x-ray sources[6–9].

Results

Strategy for the ultrafast x-ray probe. In the experiment the first x-ray pulse (400 eV, up to 10 fs long, 100 μJ/pulse) ionizes the carbon K-shell in the molecule, which, in the dominant relaxation channel, subsequently loses a second electron via Auger decay (see Fig. 1). The dication is created in a non-stationary state, a superposition of many electronic states, each with a different degree of vibrational excitation. The relaxation that follows initiates the geometry change that can lead to isomerization and molecular breakup. Upon a variable delay a second x-ray pulse, with the same characteristics as the first one, probes the instantaneous geometry in the relaxing dication by further core-ionization and Auger decay. The result is $C_2D_2^{4+}$, which has no bound states[44]. The final charge state of $4+$ is nearly impossible to reach via absorption of only one x-ray photon, and is indicative of the time dependent pump-probe dynamics. Its dissociation fragments reveal the geometry of the molecule at the probe delay time. Molecules that absorb two photons from one x-ray pulse and fragment as a tetracation contribute to a time-independent background. Alternative direct and shake ionization paths that involve the L shell of carbon typically lead to a different final charge state than the $4+$ channel. A combination of a loss of three electrons through a shake process in one step, and a loss of one electron in L-shell ionization in another step, would

lead to the final state $4+$. This combination is at least two orders of magnitude less likely than the excitation path discussed in the text.

Measurement of the momenta of all molecular fragments in coincidence as a function of time delay between the two x-ray pulses gives information about the evolution of the instantaneous molecular geometry during the relaxation of the dication. Based on total charge and momentum conservation we can separate the ion coincidences arising from the fragmentation of the tetracation from those arising from the background or the fragmentation of the molecule in other charge states. More details of the experiment and data processing can be found in Methods.

Differentiation between acetylene and vinylidene. In order to fully characterize the instantaneous molecular geometry we must detect each of the four ion fragments produced upon dissociation. In this report we discuss the time evolution of the fragmentation channel in which two deuterons and two singly charged carbon ions originating from a single $C_2D_2^{4+}$ molecule were detected. The conditions applied to identify the true $C^+/C^+/D^+/D^+$ coincidences are discussed in Methods. In order to classify the four-particle coincidences as arising from the vinylidene or the acetylene isomer, we define the angle θ:

$$\theta = \cos^{-1}\left(\frac{\text{sign}((\mathbf{p_{C_1}} - \mathbf{p_{C_2}}) \cdot \mathbf{p_{D_2}})(\mathbf{p_{C_1}} - \mathbf{p_{C_2}}) \cdot \mathbf{p_{D_1}}}{\mid \mathbf{p_{C_1}} - \mathbf{p_{C_2}} \mid\mid \mathbf{p_{D_1}} \mid}\right), \tag{1}$$

which is the angle that a deuteron momentum makes with the effective C-C axis. Here the effective C-C axis is defined by the momenta of the two heavier fragments, as the direction of the vector in

a moving frame tied to the center of mass of the two heavier particles. Vectors $\mathbf{p_{C_i}}$ and $\mathbf{p_{D_i}}$ refer to the carbon and deuteron momenta, respectively. To ensure that the vector is well-defined in a given fragmentation event, we also require that the two C^+ ions depart with momenta pointing close to 180° from each other. In other words:

$$\cos^{-1}\left(\frac{\mathbf{p_{C_1}}\cdot\mathbf{p_{C_2}}}{\mid\mathbf{p_{C_1}}\mid\mid\mathbf{p_{C_2}}\mid}\right)=\theta_{C_1-C_2}>\pi-\delta\theta_{C_1-C_2} \tag{2}$$

where $\delta\theta_{C_1-C_2}$ has the value of 1.0 rad (see Supplementary Figure 1 in for the distribution of $\theta_{C_1-C_2}$). The angle θ enables us to classify the $C^+/C^+/D^+/D^+$ coincidences as "vinylidene-like" ("V-like" further in the text) if $\theta<\frac{\pi}{2}$ (both deuteron momenta reside on the same side of the plane that divides the carbon-carbon axis). The remaining coincidences, when $\theta>\frac{\pi}{2}$, (two deuteron momenta on opposite sides of this plane) are referred to as "acetylene-like" or "A-like". The angle θ is an approximate measure of the CCD angle, because the momenta in the four-particle fragmentation are not required to point along the instantaneous directions of the molecular bonds. We point out that our labels 'A' and 'V' are defined by the directions of the particle momenta, regardless of the order in which the bonds break. Relative rotation of CCD^+ fragments can also lead to an apparent vinylidene-like angle θ.

As both the experiment reported here and that reported in Ref. [2] used non-resonant core ionization, the same dicationic state distribution is created in both experiments. By measuring the energy of the Auger electrons simultaneously, Osipov et al. concluded that the CH^+/CH^+ chan-

nel originates from excited electronic configurations of the dication, while the CH_2^+/C^+ channel comes from the $1\pi_u^{-2}$ configuration[2] (see Fig. 1). In addition, they find that CH_2^+/C^+ fragments are detected exclusively in coincidence with highest-energy Auger electrons, which indicates that isomerization does not occur in dicationic states that arise from excited configurations. We populate the same dicationic states as Osipov et al. That means that, although many excited dicationic states contribute to the $C^+/C^+/D^+/D^+$ dissociation channel in our experiment, the signal indicative of isomerization arises from the same states as discussed in the Ref. [2].

Plots of the angle θ track the differences between the V and A channels. In Fig. 2 we plot the total kinetic energy release (KER) summed over all four fragments as a function of θ integrated over the time delay. The right half of the plot contains the A-like coincidences and the left half the V-like ones. It is apparent in Fig. 2 that mean KER and the KER distribution width display a dependence on the angle θ. The mean KER value for the V-like population is several eV lower than that of the A-like population. Osipov et al. report a higher KER for the CH^+/CH^+ channel compared to that of the CH_2^+/C^+ channel in the fragmentation of the $C_2H_2^{2+}$. The same experiment reported a broader distribution of the KER in the CH^+/CH^+ channel compared to that of the CH_2^+/C^+ channel[2]. Although the energetic ordering does not have to be preserved in four-body fragmentation, Fig. 2 indicates that in case of acetylene this order is not altered. The broad distribution of the KER in the A-like channel implies that the dication is formed with significant vibrational excitation following Auger relaxation.

Time dependence in the measurement. Figure 3 shows a dependence of the deuteron

momentum distribution on the time delay between the two pulses. The deuteron momenta are represented in the center of mass frame of the two carbon ions. We choose the **x** axis along the C-C momentum difference and the component of the deuteron momentum along this direction is referred to as the parallel component. We use $\mathbf{p_{D_1}} - \mathbf{p_{D_2}}$ to define the **y** axis. Its component parallel to the C-C relative momentum is selected to be the **y** axis. The component of the deuteron momentum along **y** axis is referred to as the perpendicular component. We always select the direction of the **x** axis so that the deuteron with the smaller **y** component has a negative **x** component. With these axes the migrating deuteron is on the left and we can monitor the temporal evolution in the distribution of the average CCD molecular angle, which is reflected in the evolution of the deuteron moment distribution shown in Fig. 3.

The momentum distribution in Fig. 3 indicates that the maximum localization in both the magnitude and the angle of the deuteron momentum occurs at zero time delay (Fig. 3b). This localization is particularly pronounced for the deuteron with the smaller perpendicular component of the momentum. This observation suggests greater localization in the CD bond length and CCD angle at zero time delay. Such localization is consistent with an initial single deprotonation step in near-linear geometry. The averaged CCD angle indicates that the Auger relaxation produces vibrationally hot acetylene, predominantly sampled at turning points of the CCD bending mode. An unequal momenum peak height of the two deuterons and hence an unequal distribution width is already apparent at the nominal zero time delay, as expected for vibrationally hot sample. As the migrating deuteron on the left is more delocalized, its momentum peak height is smaller. At larger delays an increase in both the average CCD angle, as well as the spread of the CCD angles,

is evident. Although this spreading in the CCD angle is most significant at longest time delay of 100 fs where almost complete loss of localization of the deuteron momentum angle and magnitude is observed (Fig. 3f), it is important to note that the angle increase is already observable at the earliest non-zero time delay (12 fs) in the experiment (Fig. 3c).

To characterize the broadening of the proton momentum distribution, in Fig. 3h we plot the time dependence of the ratio of the signal in the region (1) to that in the area in the vicinity of the left carbon (region (2), as illustrated in Fig. 3a). Time dependence of this ratio indicates that the bending motion toward the isomerization barrier is already launched on the shortest timescale sampled by our experiment. This is consistent with the upper limit for the isomerization time reported in Ref. [1]. The increase in the bending angle at 12 fs, compared to 0 fs, is followed by a discernible decrease at 25 fs. This could be a signature of a vibrational coherence since 12 fs corresponds to one-quarter of the period of the antisymmetric bending mode in the $^1\Sigma_g^+$ state of the acetylene dication[3]. Similar evolution of the bending angle is observed in the analysis of the events where only three fragments, C^+, C^+, and D^+, are detected (see Supplementary Figure 2).

We note that the cross correlation between the two x-ray pulses can affect the zero-delay point. When both pulses arrive at the same time it is possible for a core-ionized molecule to absorb the second x-ray photon before the Auger relaxation occurs. This results in double-core hole formation, which for acetylene could be localized on the same carbon or distributed between the two carbon atoms. This manuscript concentrates on the channels in which equal sharing of the charge occurs among the four fragments, which may suppress detection of signatures of double-

core hole relaxation.

Discussion

To understand the fast onset of the isomerization, which is already apparent at the shortest delay in our experiment, we discuss in more detail the dynamics in the core-ionized acetylene ion prior to Auger relaxation. When one of the carbon atoms becomes core-ionized, the sudden change in the Coulomb field at the site of the deuterium atom bound to that carbon atom initiates motion of that deuteron. In other words, if the core-excited singly-charged ion is created in a non-stationary state it will begin to relax via a geometry change. This relaxation begins prior to interruption by the Auger relaxation. The extent of the geometry change during the core-excitation depends on the core-hole lifetime and is typically neglected in considering core-ionization[2,4,5]. This approximation is better for cases of core-excitation of nuclei with fast Auger relaxation rates as well as for heavier nuclei that experience unscreened fields. With light species, such as deuterons or protons, this geometry change during the $\sim$6 fs carbon $1s$ core hole lifetime[45] may not be negligible. Gadea et al. suggested a similar mechanism may play a role in core-to-valence excitation of acetylene[5]. Thus, if the motion on the potential energy surface of the core excited $C_2D_2^{+*}$ lasts sufficiently long, the deuterium atom adjacent to the core-excited carbon can acquire a non-negligible momentum that persists after the Auger relaxation occurs. In addition, the dication is created in an initial geometry different from that of the neutral ground state acetylene. Both the alteration in the geometry and the initial momentum can modify the path toward isomerization. Therefore, even if isomerization is incomplete during the core-hole lifetime, the molecule can be launched on the

path toward isomerization before the Auger transition occurs. Similarly, the wavepacket evolves on a mostly coulombic potential in the trication prior to the second Auger relaxation.

To test the possibility that molecular geometry changes during the core-hole lifetime, we calculated the potential energy as a function of the bending angle in the highly excited singly charged acetylene ion (see Fig. 3(i) and Supplementary Figure 3). The potential energy plot shows that the vibrational constant for the bending mode decreases in the core-excited singly charged ion, compared to the neutral. The anharmonicity of the potential energy for the core-ionized cation leads to broadening of the vibrational wavepacket as plotted in Fig. 3(i). It cannot be ruled out that this increased flexibility of the molecular bending mode contributes to a geometry change during the Auger lifetime. In the case of core-to-valence excitation of neutral acetylene[5] Gadea et al. found that both the bending mode and isomerization to vinylidene stabilize the excited state.

The singly charged core-excited ion created in a non-stationary state evolves during the core hole lifetime. The momentum that the deuterium gains during the core hole lifetime persists after the Auger decay. In addition, molecular geometry changes in the singly charged ion. This implies that Franck-Condon overlaps between the neutral and the dication will give a distorted estimate of the kinetic energy available for surmounting the isomerization barrier. In fact, it is necessary to account for both the geometry change and the acquired momentum during the core hole lifetime when considering the Franck-Condon overlaps with the dicationic states. Hence, transition-state theory applied to the dication potential energy surface without accounting for the evolution during the core hole lifetime is insufficient to describe the isomerization[2–4], because the initial state excited

by the core ionization is not static.

The new class of time-resolved x-ray pump/x-ray probe experiments reported here enables direct probing of the molecular dynamics initiated by core-ionization. By combining this technique with four-particle coincident detection, used for the first time at an x-ray FEL, we can monitor the evolving molecular geometry as a molecular movie. We applied this technique to a prototypical isomerization of the deuterated acetylene dication. We found that nonadiabatic interactions can couple nuclear motion into the electronic relaxation process in the first tens of femtoseconds following core ionization. In addition, it may be necessary to account for the geometry change that occurs during the core-excitation in order to understand the early-time dynamics in core-ionization of species that contain lighter nuclei. These findings have important implications for hydrocarbon isomerization and radiation damage by intense x-ray radiation.

Methods

Experimental design. This experiment was performed at the AMO beamline at Linac Coherent Light Source (LCLS) in the High Field Physics (HFP) chamber, which is described in detail in Ref. [13]. Pulses of x-ray radiation of 400 eV and up to 10 fs duration, 100 μJ/pulse, capable of core ionizing both the neutral and doubly ionized C_2D_2, were used in both the pump and the probe steps. The average length of the electron bunches from which the x-ray pulses were generated was 10 fs, resulting in up to 10 fs long x-ray pulses. Simulations indicate that the duration of the photon pulse can be significantly shorter than the duration of the electron bunch[46]. Our experiment, which used non-resonant excitation, is insensitive to shot-to-shot fluctuations in x-ray pulse frequency

content.

Two x-ray pulses with delays of 12, 25, 50 and 100 fs were derived from a single x-ray pulse using the split and delay apparatus described in Ref. [47]. Briefly, the apparatus consists of two mirrors in which the pitch and height of one of the mirrors can be varied. The mirror splits the pulse into two pulses that intersect at a small angle downstream. Adjusting one of the mirrors varies the difference in the path length between the two pulses and results in a variation of the time delay at the focus. In the nominal zero fs time delay, only one x-ray pulse, but with twice the fluence as the pulses at other time delays, was delivered to the sample using one of the mirrors in the split and delay apparatus. The apparatus allows for sub-femtosecond precision in setting the delay.

The two almost-collinear x-ray pulses intersect the molecular beam at a right angle. The approximate diameter of the focus was 50 μm^2. The molecular beam was produced by expanding a 1:3 mixture of C_2D_2 and He at backing pressure of 2.4 bar through an Even-Lavie pulsed valve. The sample pressure, the distance of the nozzle from the interaction region, and the photon intensity were adjusted such that on average only one molecule was fragmented per pump-probe event in order to realize unambiguous ion-coincidence measurements. The data collection rate was 120 Hz. At each time delay we analyzed $\sim 2 \cdot 10^6$ events. After filtering out false coincidences we analyzed 1087, 1307, 1137, 1392, and 1461 events at 0, 12, 25, 50, and 100 fs delay points, respectively.

Ion fragments were extracted and accelerated toward the detector using a set of parallel plates in the direction perpendicular to both the molecular beam and x-ray pulses. The ions were detected using a microchannel plate combined with a three-layer delay line anode detector (RoentDek Han-

dles GmbH HexAnode). The voltages on the spectrometer plates were set to achieve the flat-field regime. The flat-field regime permitted a straightforward reconstruction of the particle momenta along the time-of-flight direction. The other two components of the momenta, in the plane of the detector, were reconstructed by implementing the advanced reconstruction technique[48]. This technique, described in Ref. [48] benefits from the redundancy of the ion impact information collected from the three detection layers.

Momentum analysis. In order to ensure that the fragments originated from the same parent ion, two constraints were applied in the impact analysis. The first constraint requires identification of all four $C^+/C^+/D^+/D^+$ ions and up to two extra particles. The second constraint applies the conservation of momentum to the detected $C^+/C^+/D^+/D^+$ coincidence so that the sum of the four momenta is close to zero in each direction in the lab frame individually. In other words:

$$\mid p_{\mathrm{D}_{1,\mathrm{j}}} + p_{\mathrm{D}_{2,\mathrm{j}}} + p_{\mathrm{C}_{1,\mathrm{j}}} + p_{\mathrm{C}_{2,\mathrm{j}}} \mid = p_{\mathrm{j}} < \delta p_{\mathrm{j}} \tag{3}$$

where D_1, D_2, C_1, C_2 indicate the first and second deuterium and carbon atoms detected, and j is the lab frame direction. The three lab frame directions, **x**, **y**, and **z**, refer to the direction of the molecular beam, the direction of the x-ray beam propagation and the time of flight direction. The value δp_{j} is determined for each direction individually by identifying the width of the distribution of p_{j}, which was 15 au, 28 au, and 92 au for the TOF and the two in-plane directions respectively.

The final ion fragment energy was scaled by a common factor of 0.9787 determined by a calibration with CO dissociative ionization. To make this calibration we compared the measured

energies of the $2^1\Sigma^+ v = 0$ and $v = 1$ peaks in the KER spectrum of core ionized CO to those reported in the literature[49]. This scaling factor does not affect the momenta direction discussed in the manuscript.

References

1. Osipov, T. *et al.* Photoelectron-photoion momentum spectroscopy as a clock for chemical rearrangements: Isomerization of the dication of acetylene to the vinylidene configuration. *Phys. Rev. Lett.* **90** 233002 (2003).

2. Osipov, T. *et al.* Fragmentation pathways for selected electronic states of the acetylene dication. *J. Phys. B* **41** 091001 (2008).

3. Duflot, D., Robbe, J.-M. & Flament, J.-P. Ab initio study of the acetylene and vinylidene dications fragmentation. *J. Chem. Phys.* **102** 355 (1994).

4. Zyubina, T. S., Dyakov, Y. A., Lin, S. H., Bandrauk, A. D. & Mebel, A. M. Theoretical study of isomerization and dissociation of acetylene in the ground and excited electronic states. *J. Chem. Phys.* **123** 134320 (2005).

5. Gadea, F. X., Mathieu, S. & Cederbaum, L. A new perspective in X-ray induced organic chemistry: the acetylene example. *J. Mol. Struc.-Theochem.* **401** 15 (1997).

6. Chapman, H. N., Caleman, C. & Timneanu, N. Diffraction before destruction. *Phil. Trans. R. Soc. B* **369** 20130313 (2014).

7. Spence, J. C. H., Weierstall, U. & Chapman, H. N. X-ray lasers for structural and dynamic biology. *Rep. Prog. Phys.* **75** 102601 (2012).

8. Bogan, M. J. *et al.* Single particle X-ray diffractive imaging. *Nano Lett.* **8** 310 (2007).

9. Neutze, R., Wouts, R., Spel, D. v. d., Weckert, E. & Hajdu, J. Potential for biomolecular imaging with femtosecond X-ray pulses. *Nature* **406** 752 (2000).

10. Pedrini, B. *et al.* 7 Å resolution in protein two-dimensional-crystal X-ray diffraction at Linac Coherent Light Source. *Phil. Trans. R. Soc. B* **369** 20130500 (2014).

11. Caffrey, M., Li, D., Howe, N. & Shah, S. T. A. 'Hit and run' serial femtosecond crystallography of a membrane kinase in the lipid cubic phase. *Phil. Trans. R. Soc. B* **369** 20130621 (2014).

12. Bucksbaum, P. H., Coffee, R., & Berrah, N., The first atomic and molecular experiments at the Linac Coherent Light Source X-Ray free electron laser. *Adv. At., Mol., Opt. Phys.* **60** 239 (2011).

13. Bostedt, C. *et al.* Ultra-fast and ultra-intense X-ray sciences: First results from the Linac Coherent Light Source free-electron laser. *J. Phys. B: At. Mol. Opt. Phys.* **46** 164003 (2013).

14. Petrović, V. S. *et al.* Transient X-ray fragmentation: Probing a prototypical photoinduced ring opening. *Phys. Rev. Lett.* **108** 253006 (2012).

15. McFarland, B. K. *et al.* Ultrafast X-ray Auger probing of photoexcited molecular dynamics. *Nature Comm.* **5** 4235 (2014).

16. Murphy, B. F. *et al.* Femtosecond X-ray-induced explosion of C_{60} at extreme intensity. *Nature Comm.* **5** 4281 (2014).

17. Erk, B. *et al.* Imaging charge transfer in iodomethane upon X-ray photoabsorption. *Science* **345** 288 (2014).

18. Küpper, J. *et al.* X-Ray diffraction from isolated and strongly aligned gas-phase molecules with a free-electron laser. *Phys. Rev. Lett.* **112** 083002 (2014).

19. Feld, G. K. & Frank, M. Enabling membrane protein structure and dynamics with X-ray free electron lasers. *Curr. Opin. Struct. Biol.* **27** 69 (2014).

20. Neutze, R. Opportunities and challenges for time-resolved studies of protein structural dynamics at X-ray free-electron lasers. *Phil. Trans. R. Soc. B* **369** 20130318 (2014).

21. Fromme, P. & Spence, J. C. H. Femtosecond nanocrystallography using X-ray lasers for membrane protein structure determination. *Curr. Opin. Struct. Biol.* **21** 509 (2011).

22. Caleman, C. *et al.* On the feasibility of nanocrystal imaging using intense and ultrashort X-ray pulses. *ACSNano* **5** 139 (2011).

23. Park, J. *et al.* Assessment of radiation damage in single-shot coherent diffraction of DNA molecules by an extreme-ultraviolet free-electron laser. *Phys. Rev. E* **86** 042901 (2012).

24. Lorenz, U., Kabachnik, N. M., Weckert, E. & Vartanyants, I. A. Impact of ultrafast electronic damage in single-particle X-ray imaging experiments. *Phys. Rev. E* **86** 051911 (2012).

25. Seiwert, T. Y., Salama, J. K., & Vokes, E. E. The concurrent chemoradiation paradigm – general principles. *Nature Clin. Pract. Oncol.* **4** 86 (2007).

26. Domcke, W., Yarkony, D. & Köppel, H. (eds.) *Conical Intersections: Electronic Structure, Dynamics & Spectroscopy*, vol. 15 of *Advanced series in physical chemistry*, (World Scientific, 2004).

27. Jacobson, M. & Field, R. W. Acetylene at the threshold of isomerization. *J. Phys. Chem. A* **104** 3013 (2000).

28. Kellman, M. & Tyng, V. The dance of molecules: New dynamical perspectives on highly excited molecular vibrations. *Acc. Chem. Res* **40** 243 (2007).

29. Jiang, Y. H. & et al. Ultrafast extreme ultraviolet induced isomerization of acetylene cations. *Phys. Rev. Lett.* **105** 263002 (2010).

30. Laksman, J., Ceolin, D., Gisselbrecht, M., Canton, S. E. & Sorensen, S. L. Dynamics of proton migration and dissociation in core-excited ethyne probed by multiple ion momentum imaging. *J. Chem. Phys.* **131** 244305 (2009).

31. Flammini, R., Fainelli, E., Maracci, F. & Avaldi, L. Vinylidene dissociation following the Auger-electron decay of inner-shell ionized acetylene. *Phys. Rev. A* **77** 044701 (2008).

32. Alagia, M. *et al.* Angular and energy distribution of fragment ions in dissociative double photoionization of acetylene molecules at 39 eV. *J. Chem. Phys.* **136** 204302 (2012).

33. Matsuda, A., Fushitani, M., Takahashi, E. J. & Hishikawa, A. Visualizing hydrogen atoms migrating in acetylene dication by time-resolved three-body and four-body Coulomb explosion imaging. *Phys. Chem. Chem. Phys.* **13** 8697 (2011).

34. Lötstedt, E., Kato, T. & Yamanouchi, K. Intramolecular electron dynamics in the ionization of acetylene by an intense laser pulse. *J. Chem. Phys.* **138** 104304 (2013).

35. Hishikawa, A., Matsuda, A., Fushitani, M. & Takahashi, E. J. Visualizing recurrently migrating hydrogen in acetylene dication by intense ultrashort laser pulses. *Phys. Rev. Lett.* **99** 258302 (2007).

36. Hishikawa, A., Matsuda, A., Takahashi, E. J. & Fushitani, M. Acetylene-vinylidene isomerization in ultrashort intense laser fields studied by triple ion-coincidence momentum imaging. *J. Chem. Phys.* **128** 084302 (2008).

37. Adachi, J. *et al.* Photoelectron-photoion-photoion momentm spectroscopy as a direct probe of the core-hole localization in C $1s$ photoionization of C_2H_2. *J. Phys. B* **40** F285 (2007).

38. Ibrahim, H. *et al.* Tabletop imaging of structural evolutions in chemical reactions demonstrated for the acetylene cation. *Nature Comm.* **5**, 4422 (2014).

39. Alnaser, A.S. *et al.* Momentum-imaging investigations of the dissociation of D_2^+ and the isomerization of acetylene to vinylidene by intense short laser pulses. *J. Phys. B: At. Mol. Opt. Phys.* **39**, S485 (2006).

40. Janev, R. K. *Basic Properties of Fusion Edge Plasmas and Role of Atomic and Molecular Processes*, book section 1, 1–13 (Springer US, 1995).

41. Larionova, I. A., Fialkov, B. S., Kalinich, K. Y., Fialkov, A. B. & Ospanov, B. S. Ionic structure and sequence of ion formation in acetylene flames. *Combustion, Explosion and Shock Waves* **29**, 341–344 (1993).

42. Gordillo-Vázquez, F. J. & Albella, M, J. A quasianalytic kinetic model for nonequilibrium C_2H_2/H_2/Ar RF plasmas of interest in nanocrystalline diamond growth. *Plasma Sources Sci. Technol.* **11** 498 (2002).

43. Petrie, S. & Bohme, D. K. *Mass Spectrometric Approaches to Interstellar Chemistry*, vol. 225 of *Topics in Current Chemistry*, book section 2, 37–75 (Springer Berlin Heidelberg, 2003).

44. Chang, H.-B., Chen, B.-Z. & He, Y.-J. A theoretical study for the highly charged cations of C_2H_2 with and without external fields. *Acta Chim. Sinica* **66** 308 (2008).

45. Schlachter, S. *et al.* Lifetime of a K-shell vacancy in atomic carbon created by $1s \rightarrow 2p$ photoexcitation of C^+. *J. Phys. B* **37**, L103 (2004).

46. Ding, Y. *et al.* Measurements and simulations of ultralow emittance and ultrashort electron beams in the linac coherent light source. *Phys. Rev. Lett.* **102**, 254801 (2009).

47. Murphy, B. F., Castagna, J.-C., Bozek, J. D. & Berrah, N. Mirror-based soft X-ray split-and-delay system for femtosecond pump-probe experiments at LCLS. In Moeller, S. P., Yabashi, M. & Hau-Riege, S. P. (eds.) *Proc. SPIE 8504, X-Ray Free-Electron Lasers: Beam Diagnostics, Beamline Instrumentation, and Applications*, vol. 8504 850409.

48. Jagutzki, O. *et al.* Multiple hit readout of a microchannel plate detector with a three-layer delay-line anode. *IEEE Transactions on Nuclear Science* **49** 2477 (2002).

49. Lundqvist, M., Baltzer, P., Edvardsson, D., Karlsson, L. & Wannberg, B. Novel time of flight instrument for Doppler free kinetic energy release spectroscopy. *Phys. Rev. Lett.* **75** 1058 (1995).

50. Dunning, T. H., Gaussian basis functions for use in molecular calculations. I. Contraction of $(9s5p)$ atomic basis sets for the first-row atoms. *J. Chem. Phys.* **53** 2823 (1970).

Acknowledgements Portions of this research were carried out at the Linac Coherent Light Source (LCLS) at the SLAC National Accelerator Laboratory. LCLS is an Office of Science User Facility operated for the U.S. Department of Energy Office of Science by Stanford University. CELS, VSP, and PHB were supported by the National Science Foundation under Grant No. PHY-0649578. IT, TO, NB, JD, RWF, MG, AK, HL, BKM, BM, LS, SW, and TW were supported by the U.S. Department of Energy, Office of Science, Basic Energy Sciences. ASG, LJF, JPM, MS, ERS, and DW were supported by the STFC, EPSRC UK programme and ERC ASTEX. RB, CeB, BE, LF and DR were supported by Max Planck Society. DR acknowledges support from the Helmholtz Gemeinschaft through the Young Investigator Program. ChB, JDB, SC, RC, KRF, JMG, JK and MS were supported by LCLS, which is a DOE Office of Science User Facility. TJM and SM were supported by the Atomic and Molecular Optical Scisnces program within the Chemical Sciences, Geosciences, and Biosciences Division of the Office of Basic Energy Sciences, Office of Science, US Department of Energy. AR was supported by the Chemical Sciences, Geosciences, and Biosciences Division, Office of Basic Energy Sciences, Office of Science, U.S. Department of Energy. The authors would like to thank Li Fang and Ali Belkacem for stimulating discussions and Jean-Charles Castagna, Wolfram Helml, Alan Miahnahri and William White for technical assistance in preparation for the experiment.

Author Contributions VSP and PHB conceived of and designed the experiment. CELS, TO, JDB, RWF, JPM, and AR contributed to its design. VSP, CELS, TO, and PHB led the preparation and execution of the experiment. RB, ChB, JDB, SC, RC, JD, BE, KRF, JMG, HL, BM, AR, LS, MS, SW, and TW contributed to its preparation and execution. CELS and VSP lead the data analysis with help of IT, ASG, and TO. RB, CeB, BE, LF, MG, AK, JK, BKM, AN, MS, ERS, and DW contributed to the data analysis. RWF, JPM, NB, AR, DR, and LJF contributed to the discussion of the results. SM and TJM performed the electronic structure simulations. VSP, CELS, and PHB wrote the manuscript. All authors commented on the manuscript.

Competing Interests The authors declare that they have no competing financial interests.

Correspondence Correspondence and requests for materials should be addressed to Vladimir S. Petrovic (email: petrovic@slac.stanford.edu).

Figure 1 Excitation scheme. Acetylene dication states discussed in the text are given after Ref. [2]. The first x-ray pulse core ionizes the acetylene molecule, which relaxes by Auger electron emission. This process populates dicationic states, some of which are shown on the right hand side. According to Ref. [2] isomerization to vinylidene occurs on the $^1\Sigma_g^+$ potential energy surface, while acetylene-like fragmentation occurs in an excited configuration. Upon a variable delay the second x-ray pulse further core-ionizes the dication. Quadruply charged ion, formed upon the loss of the second Auger electron, dissociates and the fragment momenta are analyzed as described in the text.

Figure 2 Acetylene/vinylidene differentiation. The distribution of all $C^+/C^+/D^+/D^+$ coincidences is plotted as a function of the total kinetic energy release and the angle θ. The plot contains the data integrated over all time delays. The solid black line divides the vinylidene-like geometries (left) and acetylene-like ones (right). The data for the two isomers display a difference in both the peak KER and the width of its distribution, as shown on the right hand side.

Figure 3 Temporal evolution of the deuteron momenta. The directions parallel and perpendicular to the C-C axis are defined in (a). The measurements were done at 0 fs (b), 12 fs (c), 25 fs (d), 50 fs (e) and 100 fs (f). While the deuteron momentum distribution indicates localization in CD bond length and CCD angle at 0 fs, at longer time delays both the average CCD bending angle and the width of geometry distributions increase. Acetylene and vinylidene isomers, as well as the transition state are shown schematically

in (g). The broadening of the distribution leads to an increase in the signal in region 1 (shaded red in (a)) and a disappearance in region 2 (shaded blue in (a)). Region (1) shaded red in (a) pertains to the combinations of the deuteron momentum components where $0^\circ < tan^{-1}(p_\parallel/p_\perp) < 60^\circ$, while the region (2) pertains to $60^\circ < tan^{-1}(p_\parallel/p_\perp) < 120^\circ$. The ratio of the signal in the region 1 to that in the region 2 is shown in (h). Potential energy surfaces for the $^1\Sigma_g^+$ ground state of neutral acetylene (green) and the $^2\Sigma_u^-$ state of core-ionized cation (blue; the $^2\Sigma_g^+$ state of the core-ionized cation is almost isoenergetic) along the bending mode are shown in (i) together with the broadening of the wavefunction on the timescale of the Auger relaxation. More details about the calculation is given in the Supplemental Material.

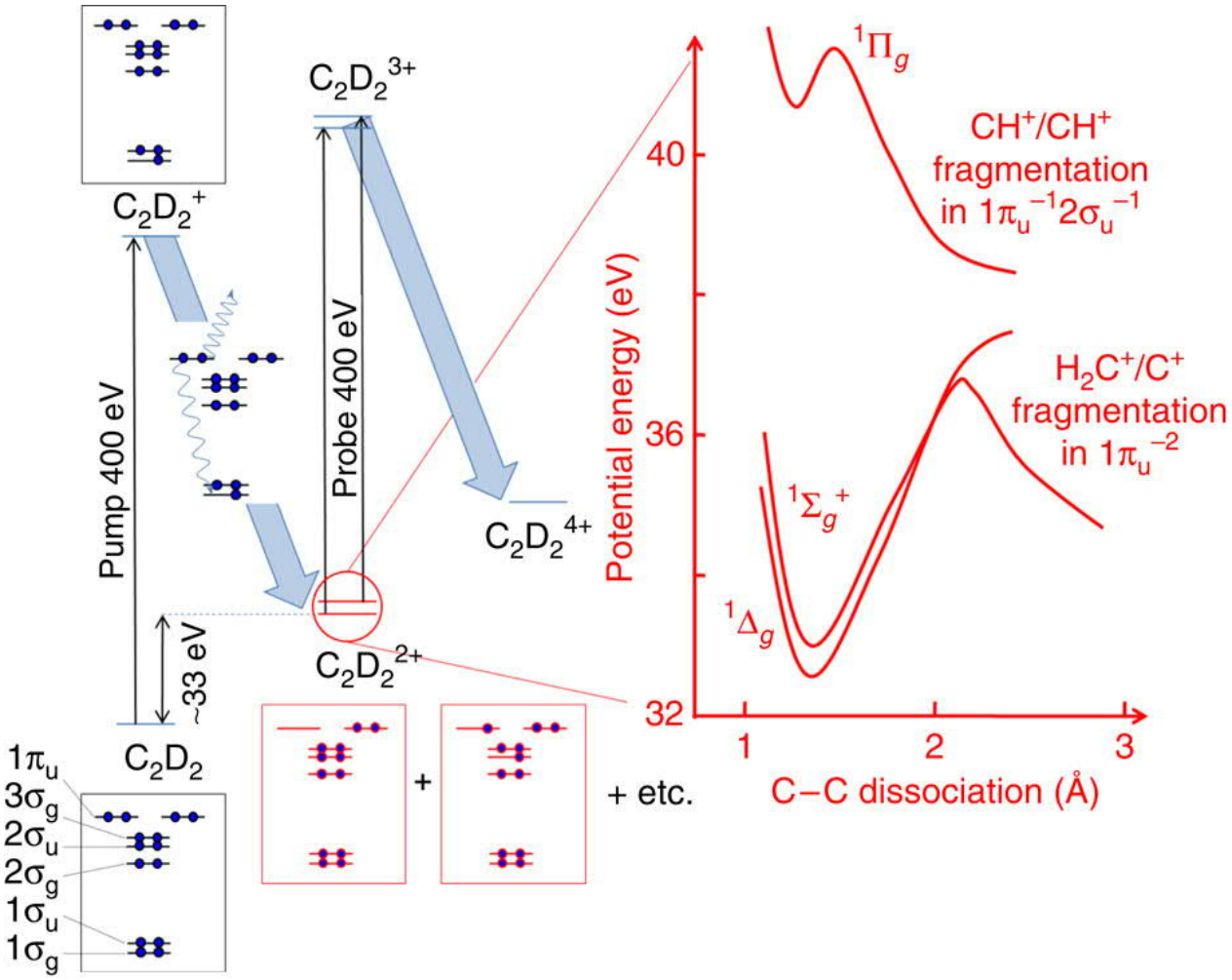
$C_2D_2^{3+}$
$C_2D_2^+$
Pump 400 eV
Probe 400 eV
~33 eV
$C_2D_2^{4+}$
$C_2D_2^{2+}$
C_2D_2
$1\pi_u$
$3\sigma_g$
$2\sigma_u$
$2\sigma_g$
$1\sigma_u$
$1\sigma_g$
+
+ etc.
Potential energy (eV)
40
36
32
1
2
3
C–C dissociation (Å)
$^1\Pi_g$
CH^+/CH^+ fragmentation in $1\pi_u^{-1}2\sigma_u^{-1}$
$^1\Sigma_g^+$
$^1\Delta_g$
H_2C^+/C^+ fragmentation in $1\pi_u^{-2}$

Figure 1.jpg

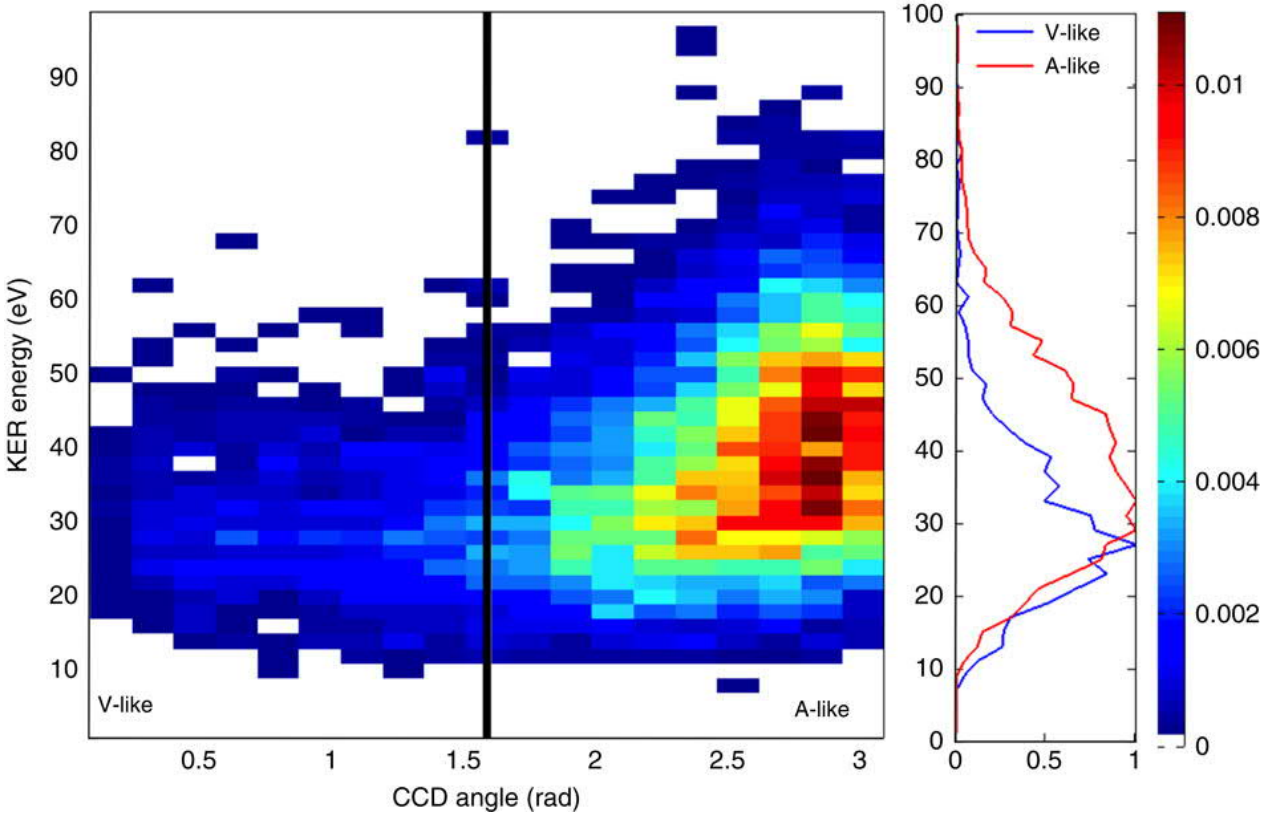
KER energy (eV)
CCD angle (rad)
V-like
A-like
V-like
A-like
0.01
0.008
0.006
0.004
0.002
0

Figure 2.jpg

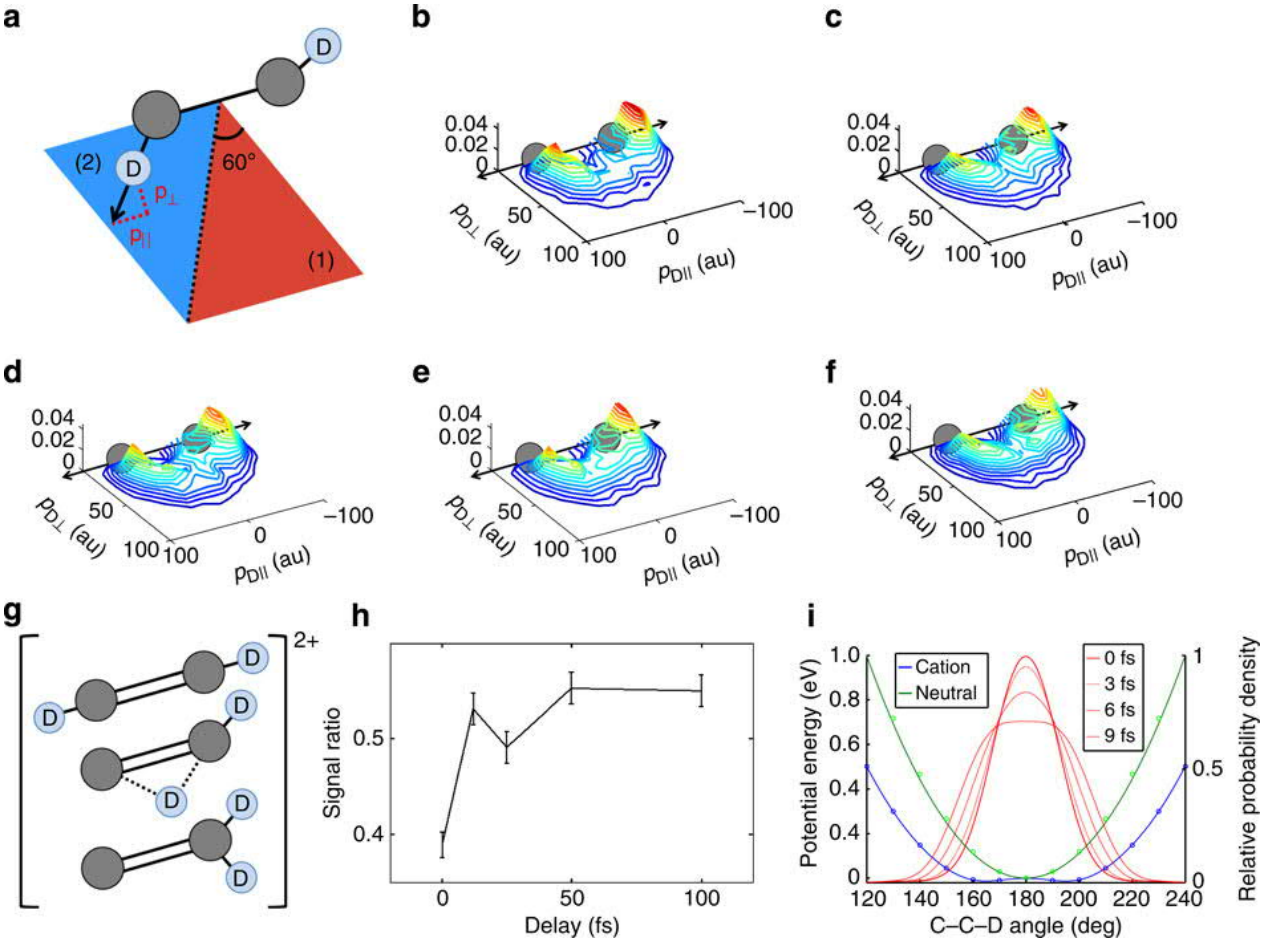
a
D
(2)
D
60°
p⊥
p||
(1)
b
0.04
0.02
0
pD⊥ (au)
50
100
100
0
−100
pD|| (au)
c
0.04
0.02
0
pD⊥ (au)
50
100
100
0
−100
pD|| (au)
d
0.04
0.02
0
pD⊥ (au)
50
100
100
0
−100
pD|| (au)
e
0.04
0.02
0
pD⊥ (au)
50
100
100
0
−100
pD|| (au)
f
0.04
0.02
0
pD⊥ (au)
50
100
100
0
−100
pD|| (au)
g
2+
D
D
D
D
D
D
h
Signal ratio
0.5
0.4
0
50
100
Delay (fs)
i
Potential energy (eV)
1.0
0.8
0.6
0.4
0.4
0
Cation
Neutral
0 fs
3 fs
6 fs
9 fs
1
0.5
0
Relative probability density
120
140
160
180
200
220
240
C–C–D angle (deg)

Figure 3.jpg

Supplementary Figures

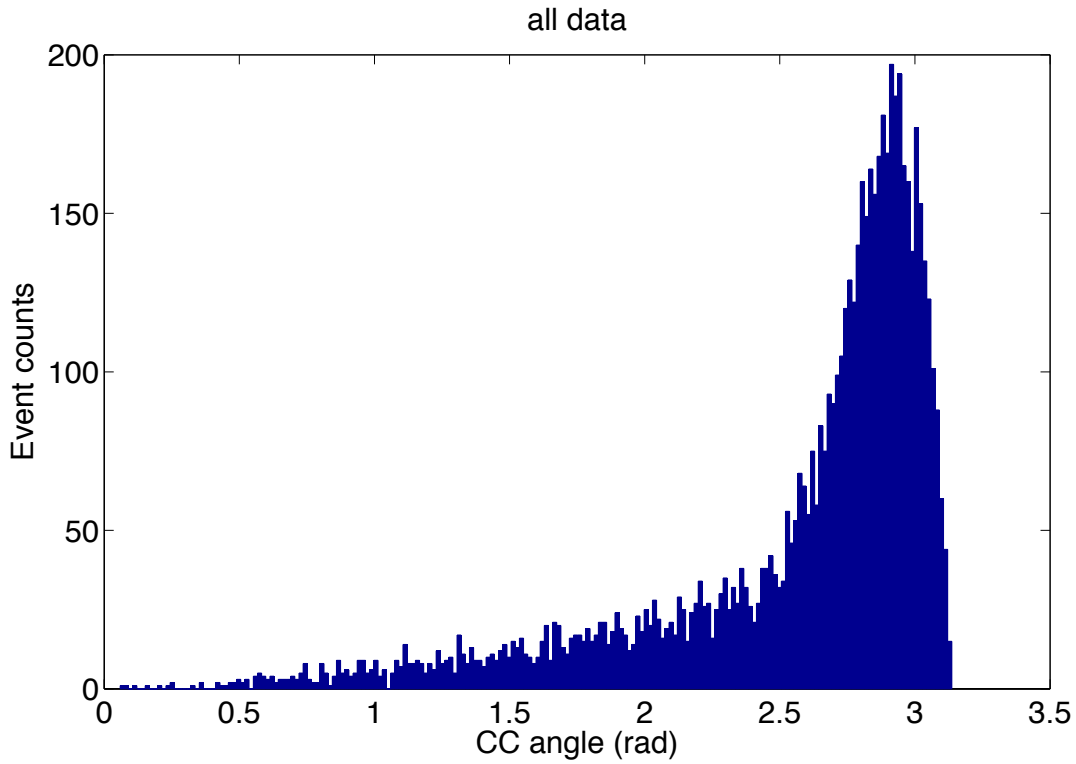

Supplementary Figure 1. Carbon fragment momenta. Plotted is the distribution of angles among the two carbon fragments defining the effective C-C axis.

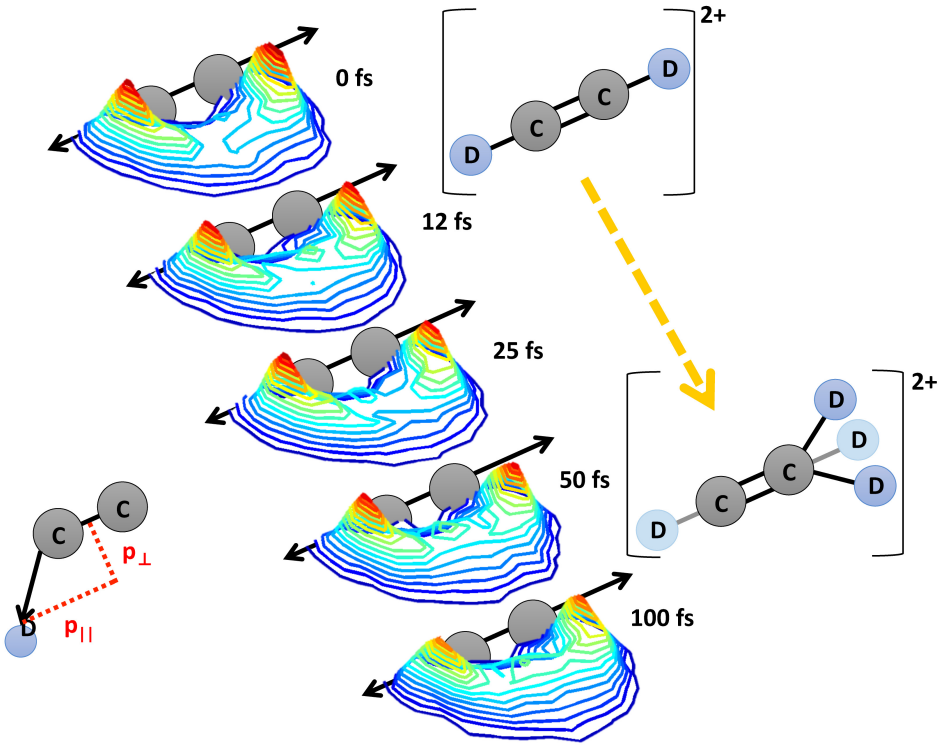

Supplementary Figure 2. Temporal evolution of the deuteron momenta in three-particle coincidences. Similar to Fig. 3 in the main text, but for events in which only three particles, C^+, C^+, and D^+, are detected: temporal evolution of the distribution of the deuteron momentum components parallel and perpendicular to the C-C axis at 0 fs (a), 12 fs (b), 25 fs (c), 50 fs (d) and 100 fs (e). Three particles are detected more often than all four, resulting in a larger number of events for analysis. However, with only three particles the requirement that the momentum sum is near zero cannot be used as a filter. This leads to a larger dilution of the signal with false coincidences as compared to Fig. 3.

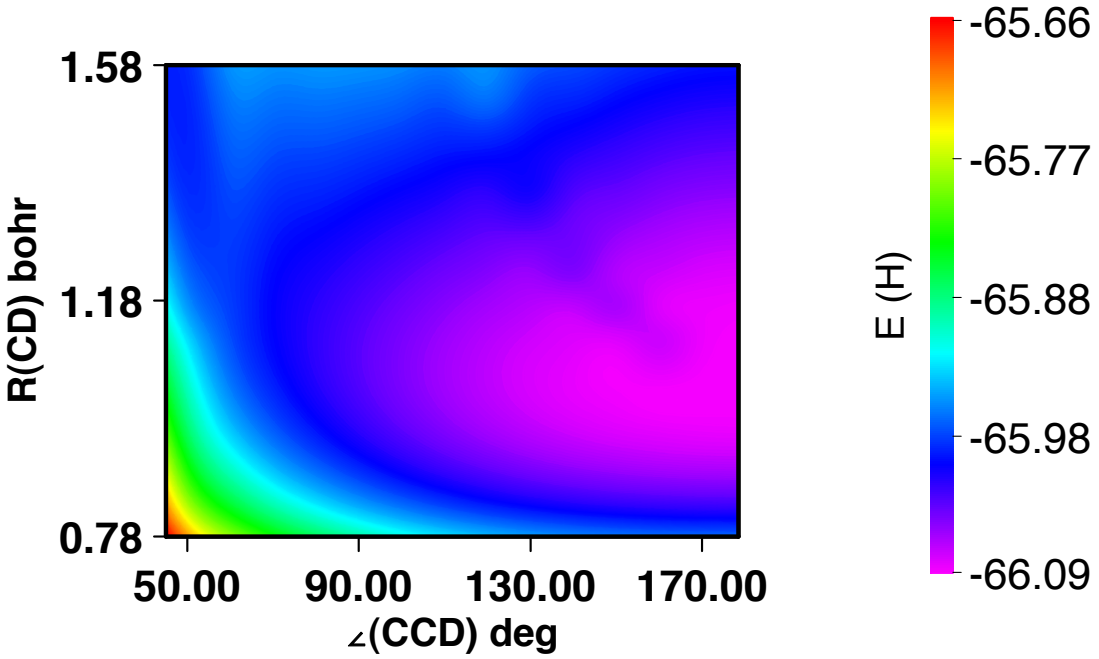

Supplementary Figure 3. Potential energy surface of the $^2\Sigma_u^-$ state of the 1s core-ionized $C_2D_2^{+*}$ Potential energy is plotted as a function of the CCD bending angle and the CD internuclear distance ($^2\Sigma_g^+$ is almost isoenergetic; comparison to the potential energy of the $1\Sigma_g^+$ ground state of neutral given is in the main text, Fig. 3(i)). The potential energy surface of C_2D_2 was obtained at the Hartree-Fock (HF) level of theory using Dunning's double-zeta basis (DZP) [1]. For $C_2D_2^+$ we first carried out the HF/DZP calculation on the C_2D_2 ground state. We then started with two reference ion configurations, ($1a'^1 2a'^2 3a'^2 4a'^2 5a'^2 1a''^2 2a''^2$) and ($1a'^2 2a'^1 3a'^2 4a'^2 5a'^2 1a''^2 2a''^2$), with a single vacancy in the C1s orbital, and performed an all-singles configuration-interaction calculation, constraining the maximum combined electron occupancy of the core molecular orbitals, 1a' and 2a', to three. Note that the bond distances and angles, other than those being plotted, are fixed at the equilibrium geometry of the neutral C_2D_2. Evolution of the molecular geometry begins on this potential energy surface prior to Auger relaxation. Increased flexibility of the bending mode in core-ionized acetylene could facilitate geometry change during the Auger lifetime. Auger lifetime of the 1s hole in carbon is approximately 6 fs [2].

Supplementary References

[1] Dunning, T. H., Gaussian basis functions for use in molecular calculations. I. Contraction of (9s5p) atomic basis sets for the first-row atoms. J. Chem. Phys. 53 2823 (1970).
[2] Schlachter, S. et al. Lifetime of a K-shell vacancy in atomic carbon created by 1s → 2p photoexcitation of C^+. J. Phys. B 37, 103 L103 (2004).